Increasing Enantioselectivities and Reactivities by Stereochemical Tuning: Fenchone-Based Catalysts in Dialkylzinc Additions to Benzaldehyde

Bernd Goldfuss,*[a] Melanie Steigelmann,[a] and Frank Rominger[+]

Dedicated to Professor Paul von Ragué Schleyer on the occasion of his 70th birthday

Keywords: Asymmetric synthesis / Zinc / Transition structures / QM/MM computations

Trimethylsilyl substitutions of the fenchyl alcohols [(1*R*,2*R*,4*S*)-*exo*-(2-Ar)-1,3,3-trimethylbicyclo[2.2.1]heptan-2-ol, Ar = 2-methoxyphenyl (**1**) and Ar = 2-(dimethylaminomethyl)phenyl (**2**)] yield the chiral ligands **3** [Ar = 2-methoxy-3-(trimethylsilyl)phenyl] and **4** [Ar = 2-(dimethylaminomethyl)-3-(trimethylsilyl)phenyl]. Increased reactivities and enantioselectivities in diethylzinc additions to benzaldehyde are obtained from **3** (63% *ee R*) and **4** (93% *ee S*), relative to **1** (26% *ee S*) and **2** (73% *ee S*). X-ray crystal structures of **3** and of its methylzinc complex **3-Zn** reveal out-of-plane bending of the methoxy groups as major geometrical consequences of the trimethylsilyl substitutions. Analyses of QM/MM ONIOM μ-O transition-structure models for **1**, **2**, **3**, and **4** show that trimethylsilyl-induced distortions of methoxy and of dimethylaminomethyl groups explain the observed increased enantioselectivities.

Introduction

Enantioselective 1,2-additions of organozinc reagents[1] to prochiral carbonyl[2] and imino[3] systems are fundamental tools for the synthesis of optically active compounds,[4] and the design of chiral promoters for these processes is of central interest.[5] A huge number of chiral ligands has been applied in enantioselective additions of organozinc compounds to aldehydes,[5,6] but efficient ligands with short synthetic routes are still desirable. The underlying origins for directions and relative degrees of enantioselectivities in dialkylzinc additions to aldehydes are puzzling.[7]

Qualitative mechanistic understanding and quantitative rationalization of enantioselection processes can provide a basis for rational catalyst design. We have recently shown that μ-O transition-structure models can be successfully employed to understand enantioselectivities of dialkylzinc additions to benzaldehyde (Scheme 1), catalyzed by chiral β-amino alcohols, e. g., proline and 1,2-diphenylethane derivatives.[8]

Bicyclic terpenes (e.g., camphor and fenchone) are valuable sources for the construction of chiral ligands and catalysts,[9] and Noyori et al. have proven that 3-*exo*-(dimethylamino)isonorborneol (DAIB) is among the best.[10] Chelating fenchyl alcohols are readily accessible by organolithium additions to fenchone, but only moderate enantioselectivities (up to 64% *ee*) were reported for catalyzed diethylzinc additions to benzaldehyde.[9b]

We here present a combined experimental and computational study of fenchone-based catalysts, whose enantioselectivities and reactivities in diethylzinc additions to benzaldehyde were investigated. Significantly improved enantioselectivities and increased reactivities were obtained by stereochemical tuning. X-ray crystal structures and computational analyses were employed to interpret and rationalize the results of the catalytic reactions.

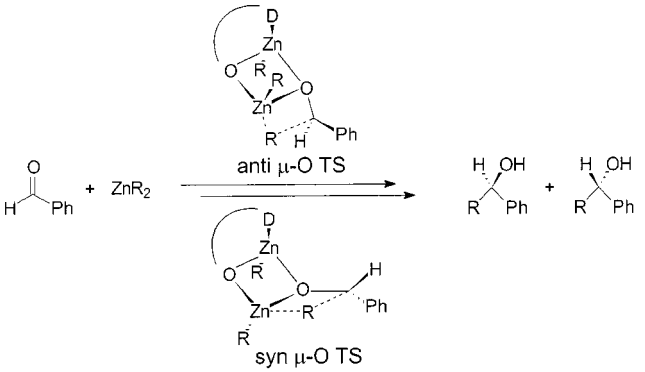

Scheme 1. Enantioselective dialkylzinc addition to benzaldehyde via *anti*- and *syn*-μ-O transition structures; the O∪D units designate chiral, donor (D) functionalized chelate ligands

Results and Discussion

Synthesis and Structural Characterization of the Ligands

Modular ligand systems are highly appreciated in enantioselective catalysis, due to their high degree of variability.[6,11] With chelating fenchyl alcohols, variations of coordination donor functions (e.g., OMe, CH_2NMe_2, Scheme 2) are easily accessible;[12] this enables tuning of the stereochemical outcome of enantioselective diethylzinc additions.[13] Substituents (X, e.g., $SiMe_3$) in *ortho* positions of the aryl moieties (Scheme 2) should even further influence reactivities and enantioselectivities of the catalysts.[14]

[a] Organisch-Chemisches Institut der Universität Heidelberg, Im Neuenheimer Feld 270, 69120 Heidelberg, Germany
E-mail: Bernd.Goldfuss@urz.uni-heidelberg.de
[+] X-ray analyses.

  1434−193X/00/0509−1785 $ 17.50+.50/0

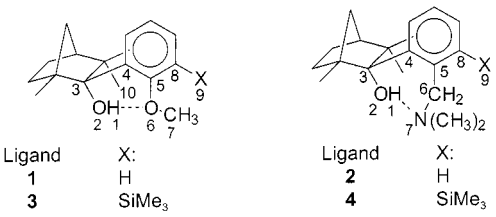

Scheme 2. Chelating fenchyl alcohols

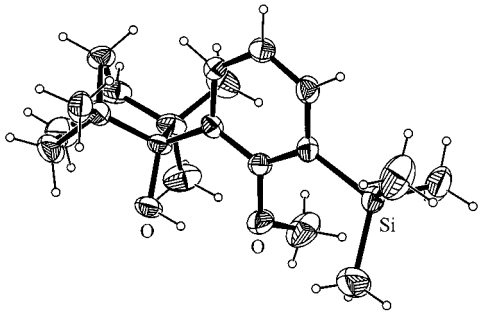

Figure 1. X-ray crystal structure of **3**

Geometrical effects of the *ortho*-trimethylsilyl substituents are indeed apparent from comparisons of X-ray crystal structures of the ligands **1** (X = H) and **3** (X = $SiMe_3$, Scheme 2, Figure 1). While the methoxy group is aligned coplanar with the aryl moiety in **1** (C7–O6–C5–C8: –3°, Table 1), trimethylsilyl substitution forces the methyl group to bend out of the aryl plane in **3** (C7–O6–C5–C8: –72°, Table 1). This alignment reduces repulsion between C7 and C8 (2.81 Å in **1**, 3.05 Å in **3**) and hence results in a smaller O6–C5–C8 angle in **3** (118°) than in **1** (123°, Table 1). However, repulsive interactions arise from close contacts between the geminal dimethyl unit (C10, Scheme 2) of the bicycloheptane moiety and the out-of-plane bent C7 in **3** (3.66 Å) relative to **1** (4.29 Å). This results, by rotation of the C3–C4 axis, in a more coplanar arrangement of the O2–C3–C4–C5 unit (33° in **3**, 47° in **1**, Table 1). Hence, trimethylsilyl substitution of **1** significantly alters the HO∪OMe alignment in **3**.

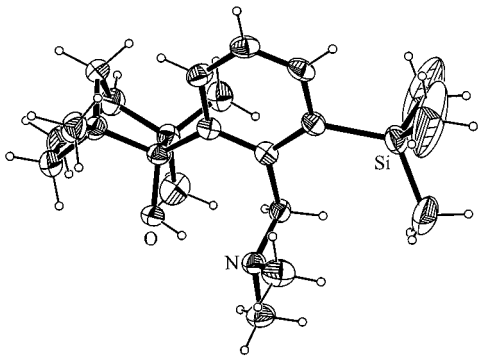

Figure 2. X-ray crystal structure of **4**

A comparison of the X-ray crystal structures of **2** (X = H) and **4** (X = $SiMe_3$, Scheme 2, Figure 2) shows a small decrease of the C4–C5–C6 angle (126° in **2**, 121° in **4**) and a slight increase of the C6–C5–C8 angle (116° in **2** and 118° in **4**) upon trimethylsilyl substitution (Table 2). The O2–C3–C4–C5 segment is less coplanar in **4** (49°) than in **2** (43°). The N7–C6–C5–C8 dihedral angle of **4** is not larger than that of **2** (both 110°, Table 2).[15]

Reactivity and Enantioselectivity of the Catalysts

The chiral 1,3,3-trimethylbicyclo[2.2.1]heptane moieties, the heteroatom donor groups and the chelate ring sizes[16] are all identical for the pair **1** and **3** and the pair **2** and **4** (Scheme 2). The trimethylsilyl substituents of **3** and **4** make them more reactive (increased chemical yield) than **1** and **2**, respectively (Table 3). Furthermore, the degrees of enantioselectivity of **3** and **4** are greater than those of **1** and **2**, respectively (Table). Even the direction of enantioselectivity of **3** (*R* product) and **1** (*S* product) differ.

Why do trimethylsilyl substituents in the remote *ortho* position of **3** increase the reactivity relative to **1** (Scheme 2)? Elaborate investigations by Noyori et al. on DAIB-catalyzed dialkylzinc additions to benzaldehyde revealed that *monomeric* zinc chelate complexes are the active catalysts for dialkylzinc additions to aldehydes, while the dimers are unreactive.[17] The monomer–dimer equilibrium of zinc chelate complexes determines the appearance of the mono-

Table 1. X-ray crystal structural data of chelating fenchyl alcohols **1**[13] and **3** (see Scheme 2); distances in Å, angles in °

	H1–O6	O2–O6	O2–C3–C4	C4–C5–O6	O6–C5–C8	C5–C8–X9	O2–C3–C4–C5	C7–O6–C5–C8
1[a]	1.94	2.62	108	116	123	120	47	–3
3	1.86	2.60	109	119	118	127	33	–72

[a] Average values of four independent molecules of **1**.

Table 2. X-ray crystal structural data of fenchyl alcohols **2**[13] and **4** (see Scheme 2); distances in Å, angles in °

	H1–N7	O2–N7	O2–C3–C4	C5–C8–H9	C4–C5–C6	C6–C5–C8	O2–C3–C4–C5	N7–C6–C5–C8
2	1.69	2.66	108	120	126	116	43	110
4	1.80	2.64	111	129	121	118	49	110

Table 3. Enantioselective additions of diethylzinc to benzaldehyde; in hexanes, 3 mol-% ligand was employed

Ligand	*T* [°C]	Reaction time [h]	Chemical yield[a]	Enantiomer[b]	%ee [c]
1[d]	–30	24	56%	*S*	26
2[d]	+6	24	57%	*S*	73
3	–30	24	66%	*R*	63
4	+6	24	79%	*S*	93

[a] The completion of reaction was monitored by GC analysis. – [b] Major enantiomer of the 1-phenyl-1-propanol product. – [c] Enantiomeric excess, chiral HPLC analyses. – [d] See ref.[13]

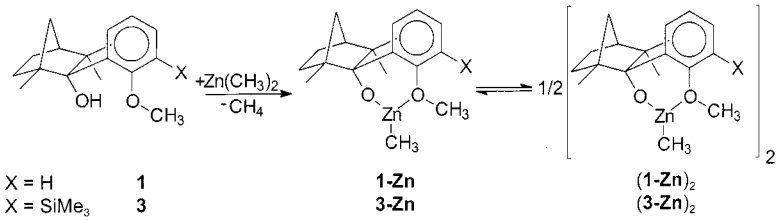

Scheme 3. Synthesis and monomer–dimer equilibrium of methylzinc chelate complexes

meric species and hence influences the reactivity. This equilibrium (shown in Scheme 3 for methylzinc complexes of **1** and **3**) is also crucial for asymmetric amplification phenomena.[18]

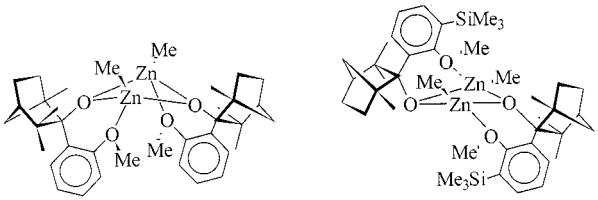

Scheme 4. Structures of $(\mathbf{1\text{-}Zn})_2$ [19] and $(\mathbf{3\text{-}Zn})_2$

We recently reported the X-ray crystal structure of the dimeric methylzinc chelate complex $(\mathbf{1\text{-}Zn})_2$ (Scheme 4, Figure 3),[19] which is the methyl analog of the ethylzinc catalyst of **1** (employed for the catalytic experiments, Table 3). Complex $(\mathbf{1\text{-}Zn})_2$ has *syn*-aligned methylzinc moieties (Figure 3), analogous to Noyori's homochiral *syn*-methylzinc DAIB complex.[18b]

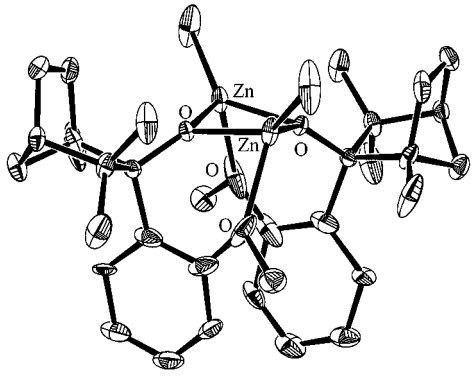

Figure 3. X-ray crystal structure of $(\mathbf{1\text{-}Zn})_2$ [19]

Computational evaluations assess the degree of dimer formation in the monomer–dimer equilibria of the methylzinc catalysts **1-Zn** and **3-Zn** (Scheme 3).[20] In agreement with the higher reactivity of **3-Zn** (Table 3), the dimerization energy for **3-Zn** (21.0 kcal/mol) is 11.3 kcal/mol smaller than for **1-Zn** (32.3 kcal/mol). The increased tendency of $(\mathbf{3\text{-}Zn})_2$ towards dissociation is apparently geometrically determined, and is shown by larger external (dimer-forming) Zn–O distances [2.21 Å in $(\mathbf{3\text{-}Zn})_2$ vs. 2.13 Å in $(\mathbf{1\text{-}Zn})_2$] of the central Zn_2O_2 rings, shorter internal Zn–O bonds [1.88 Å in $(\mathbf{3\text{-}Zn})_2$ vs. 1.91 Å in $(\mathbf{1\text{-}Zn})_2$] and longer aryl–aryl distances [3.72 Å in $(\mathbf{1\text{-}Zn})_2$ vs. 5.09 Å in $(\mathbf{3\text{-}Zn})_2$] (Figure 4, 5).

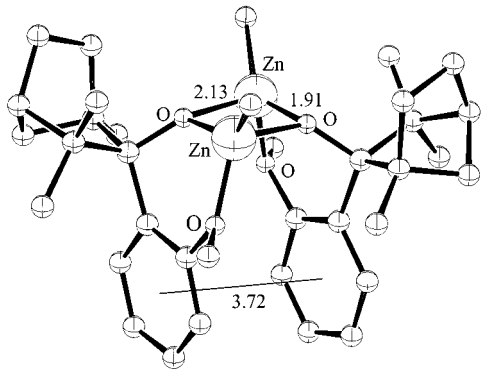

Figure 4. ONIOM (RHF/LanL2DZ:UFF) optimized structure of $(\mathbf{1\text{-}Zn})_2$

Synthesis and X-ray crystal analysis of trimethylsilyl-substituted **3-Zn** reveals the formation of dimeric $(\mathbf{3\text{-}Zn})_2$ (Figure 6), in analogy to dimeric $(\mathbf{1\text{-}Zn})_2$ (Scheme 4). Significant geometrical differences are, however, apparent in $(\mathbf{3\text{-}Zn})_2$ relative to $(\mathbf{1\text{-}Zn})_2$. In contrast to the *syn* alignments of methylzinc groups in the X-ray crystal structure of $(\mathbf{1\text{-}Zn})_2$,[19] *anti* orientations of methylzinc groups are apparent in $(\mathbf{3\text{-}Zn})_2$ (Figure 6).

Complex $(\mathbf{1\text{-}Zn})_2$ exhibits short Zn–O(Me) contacts of 2.19 Å.[19] In $(\mathbf{3\text{-}Zn})_2$, the Zn–O(Me) distance (2.40 Å) is long due to repulsion between synperiplanar aligned methyl groups at oxygen and zinc (C–O–Zn–C: 2°, C–C: 3.41 Å), while a shorter Zn–O(Me) contact (2.27 Å) arises from an antiperiplanar methoxy and methylzinc group arrangement (C–O–Zn–C: 173°). The aryl–methoxy group coplanarity (measured by the C7–O6–C5–C8 dihedral angle, Scheme 2)

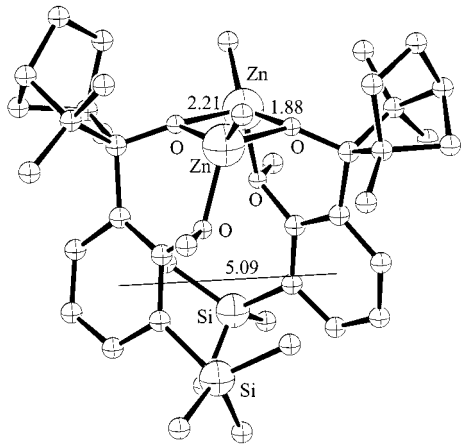

Figure 5. ONIOM (RHF/LanL2DZ:UFF) optimized structure of $(\mathbf{3\text{-}Zn})_2$ [20]

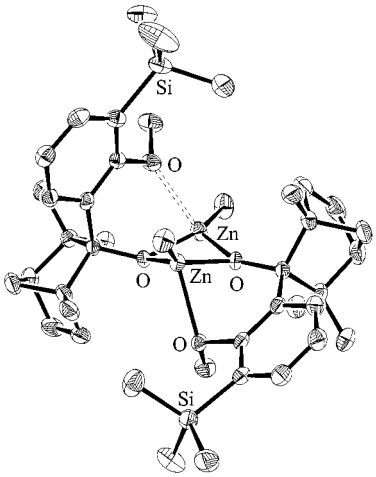

Figure 6. X-ray crystal structure of $(\mathbf{3\text{-}Zn})_2$

in $(\mathbf{3\text{-}Zn})_2$ is –101° for the methoxy group with the larger (2.40 Å) Zn–O distance and –56° for the methoxy group with the shorter (2.27 Å) contact to Zn. As in the X-ray crystal structure of **3** (Figure 1), close distances between the methoxy methyl groups and the geminal dimethyl moiety of the bicycloheptane unit are apparent in $(\mathbf{3\text{-}Zn})_2$ (C–C: 3.55 Å). The in-plane aligned methoxy group in $(\mathbf{1\text{-}Zn})_2$[19] gives rise to much longer distances (C–C: 3.85 Å). The internal Zn–O bonds of the central Zn_2O_2 rings of $(\mathbf{1\text{-}Zn})_2$ (1.97 Å) and $(\mathbf{3\text{-}Zn})_2$ (1.95, 1.98 Å) are similar, while the external (dimer-forming) Zn–O bonds are shorter in $(\mathbf{1\text{-}Zn})_2$ (2.01 Å) than in $(\mathbf{3\text{-}Zn})_2$ (2.02, 2.04 Å). This reflects the greater tendency of $(\mathbf{3\text{-}Zn})_2$ to dissociate more readily into reactive monomers **3-Zn**, and agrees with the higher reactivity of **3** relative to **1** in diethylzinc additions to benzaldehyde.[21]

How do the trimethylsilyl substituents of **3** and **4** influence the enantioselectivities in diethylzinc additions to benzaldehyde? The experimental enantioselectivities (Table 1) can be reproduced[22] and can be explained computationally by μ-O transition-structure models,[8,23] if four μ-O transition-structure types with *anti*- and *syn*-aligned methylzinc groups, yielding *R*- and *S*-configured products (Scheme 5), are used.

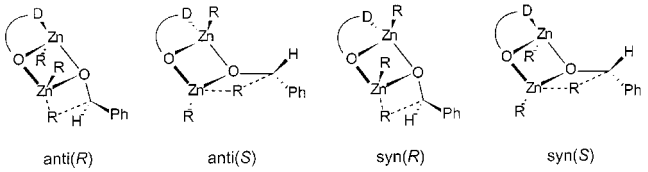

Scheme 5. Computed *anti*- and *syn*-μ-O transition structures; the O∪D unit denotes the chelating ligand with an OMe donor group (D) for **1** and **3** and a CH_2NMe_2 donor (D) for **2** and **4**

S-Configured 1-phenyl-1-ethanol (as model for the experimental 1-phenyl-1-propanol) is produced by ligands **1** and **2** via the lowest-energy transition structures **1**-*syn* (*S*) and **2**-*anti* (*S*) (Table 4). The computed direction and the lower enantioselectivity for **1** [0.4 kcal/mol energy difference, ΔE, between **1**-*syn* (*S*) and **1**-*anti* (*R*)] relative to **2** [ΔE = 2.5 kcal/mol between **2**-*anti* (*S*) and **2**-*syn* (*R*)] correspond with the experimental results (Table 3).

Table 4. Computed (RHF/LanL2DZ:UFF) total (a.u.) and relative (kcal/mol) energies of μ-O-*syn* and -*anti* transition structures (Scheme 5); transition structure optimizations and frequency analyses were performed by ONIOM (RHF/LanL2DZ:UFF) computations; a single imaginary frequency corresponds in all cases to methyl transfer from zinc to the aldehyde carbon atom; the lowest energy transition structure (in bold and italics typeface) determines the configuration of the product and the energy difference to the next stable transition structure (bold typeface) is used as a measure for enantioselectivity

Ligand	*anti* (*R*)	*anti* (*S*)	*syn* (*R*)	*syn* (*S*)
1	–434.91175	–434.89675	–434.88393	–434.91230
rel.	**0.4**	9.8	17.8	***0.0***
2	–434.89222	–434.89707	–434.89304	–434.88370
rel.	3.0	***0.0***	**2.5**	8.4
3	–434.89995	–434.88229	–434.87976	–434.89822
rel.	***0.0***	11.1	12.7	**1.1**
4	–434.87761	434.88745	–434.88217	–434.87086
rel.	6.2	***0.0***	**3.3**	10.4

Trimethylsilyl substitution of **1** changes the direction of enantioselectivity for **3**, both experimentally (Table 3) and computationally (Table 4): the most stable transition structure changes from **1**-*syn* (*S*) to **3**-*anti* (*R*). Formation of (*R*)-1-phenyl-1-ethanol via **3**-*anti* (*R*) is more favorable (ΔE = 1.1 kcal/mol) for **3** than generation of the *S* product via **3**-*syn* (*S*) (ΔE = 0.4 kcal/mol, Table 4). This increased preference of **3** for the *R* product is in agreement with experimental enantioselectivities (Table 3).

Superpositions show how trimethylsilyl substitutions stabilize **3**-*anti* (*R*) and destabilize **3**-*syn* (*S*) relative to the analogous structures of **1** (Figure 7 and Figure 8). The transition structures reveal distortions of **3**-*syn* (*S*) and of **3**-*anti* (*R*) relative to **1**-*syn* (*S*) and **1**-*anti* (*R*).

These distortions move the aldehyde carbon atom away from the transferring methyl group in **3**-*syn* (*S*), but compress electrophilic and nucleophilic parts in **3**-*anti* (*R*). The methyl transfer is favored more on the side of the Zn_2O_2 ring which is opposite to the trimethylsilyl group in **3**-*anti* (*R*). As in the X-ray crystal structures of **3** and of $(\mathbf{3\text{-}Zn})_2$ (Figure 1 and Figure 6), the distortions arise from trime-

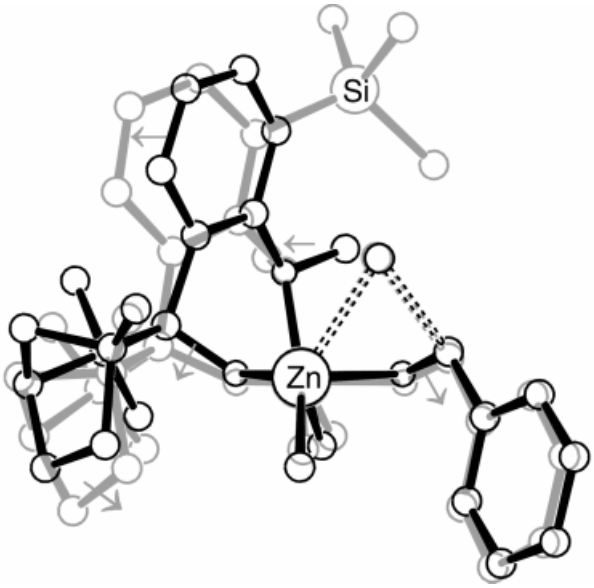

Figure 7. Superposition of **1**-*syn* (*S*) (black) and **3**-*syn* (*S*) (gray) transition structures; zinc atoms are eclipsed and hydrogen atoms are omitted for clarity

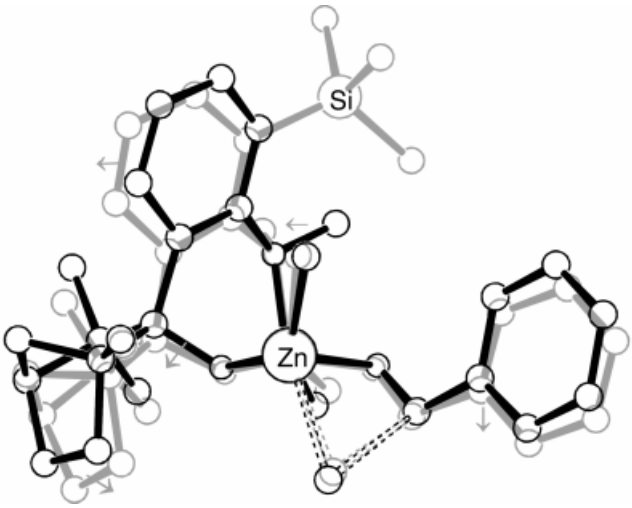

Figure 8. Superposition of **1**-*anti* (*R*) (black) and **3**-*anti* (*R*) (gray) transition structures; zinc atoms are eclipsed and hydrogen atoms are omitted for clarity

thylsilyl-induced out-of-plane bending of methoxy groups and repulsion with geminal dimethyl units of the bicycloheptane moieties [C–C: **3**-*syn* (*S*) 3.96 Å, **1**-*syn* (*S*) 4.54 Å; **3**-*anti* (*R*) 3.95 Å, **1**-*anti* (*R*) 4.59 Å] and explain the observed enantioselectivities (Table 3).

Trimethylsilyl substitution of **2** increases the enantioselectivity of the *R* product for **4**, both experimentally (73 to 93% *ee*, Table 3) and computationally. The energy difference is increased from 2.5 kcal/mol between **2**-*anti* (*S*) and **2**-*syn* (*R*) to 3.3 kcal/mol in the analogous *anti* (*S*) and *syn* (*R*) transition structures of **4** upon trimethylsilyl substitution (Table 4).

Superpositions of **2**,**4**-*anti* (*S*) and of **2**,**4**-*syn* (*R*) show distortions upon trimethylsilyl substitution (Figure 9 and Figure 10). Similar to transition structures of **1** and **3** (Figure 7 and Figure 8), methyl transfer becomes more favored on the side of the Zn_2O_2 core which is opposite to the trimethylsilyl group.

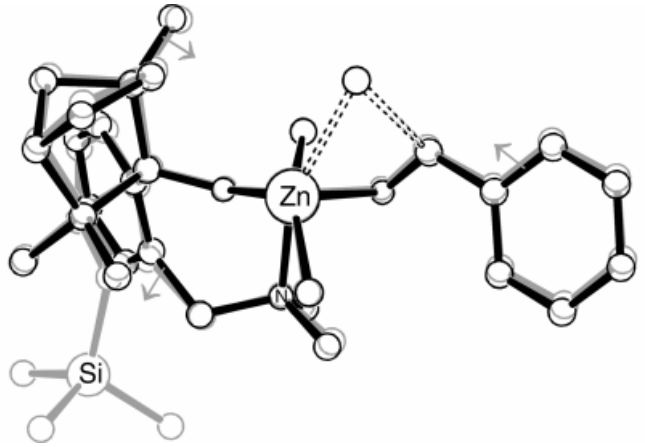

Figure 9. Superposition of **2**-*anti* (*S*) (black) and **4**-*anti* (*S*) (gray) transition structures; zinc atoms are eclipsed and hydrogen atoms are omitted for clarity

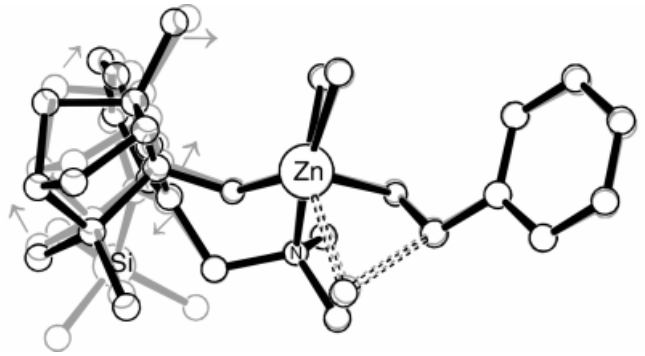

Figure 10. Superposition of **2**-*syn* (*R*) (black) and **4**-*syn* (*R*) (gray) transition structures; zinc atoms are eclipsed and hydrogen atoms are omitted for clarity

The trimethylsilyl-induced distortions originate from increased N7–C6–C5–C8 dihedral angles [Scheme 2, 105° in **4**-*anti* (*S*) vs. 97° in **2**-*anti* (*S*); 105° **4**-*syn* (*R*) vs. 95° in **2**-*syn* (*R*)],[15] and give rise to the observed increased enantioselectivity of the *S* product by **4** relative to **2** (Table 3).

Conclusions

The introduction of trimethylsilyl groups in the *ortho* positions of the fenchyl alcohols **1** and **2** alters the direction (for **3**) and increases the degree of enantioselectivity as well as the reactivity (for **3** and **4**) in diethylzinc additions to benzaldehyde. X-ray crystal structure analysis shows that trimethylsilyl substitution induces reorientation of the methoxy group in **3**. Computational analyses of dimeric methylzinc chelate complexes of **1** and **3** show that **3-Zn** has a greater tendency to dissociate into reactive monomers than **1-Zn** has; this agrees with the higher experimental reactivity of **3** relative to **1**. The different natures of **1** and **3** are also apparent from the geometries of the X-ray crystal structures of $(\mathbf{3\text{-}Zn})_2$ and $(\mathbf{1\text{-}Zn})_2$. The experimental trends of the enantioselectivities in diethylzinc additions to benzaldehyde are reproduced by μ-O transition structure models.

Analyses of the transition structures show that trimethylsilyl substitutions induce reorientations of methoxy and of dimethylaminomethyl groups. The observed enantioselectivities arise from these distinct stereochemical effects. Larger substituents than trimethylsilyl (e.g., triphenylsilyl or triisopropylsilyl) might lead to even stronger effects and result in higher reactivities and enantioselectivities in dialkylzinc additions to aldehydes.

Experimental Section

General: The reactions were carried out under argon (Schlenk and needle-septum techniques) with dried and degassed solvents. – X-ray crystal analyses were performed with a Bruker Smart CCD diffractometer. – NMR spectra were recorded with a Bruker AMX300 spectrometer. – IR spectra were run with a Bruker Equinox 55 FT-IR spectrometer. – Optical rotations were measured with a Perkin–Elmer P241 machine. – GC analyses were carried out with a Chrompack (CP9001) and HPLC analyses on a HP-1100 machine with a Chiracel OB-H column. – For the synthesis of **1** and **2**, see ref.[13] – Crystallographic data (excluding structure factors) for the structures reported in this paper were deposited with the Cambridge Crystallographic Data Centre as supplementary publication nos. CCDC-135946 to -135948. Copies of the data can be obtained free of charge on application to: CCDC, 12 Union Road, Cambridge CB2 1EZ, UK [Fax: (int.) + 44-1223/336-033; E-mail: deposit@ccdc.cam.ac.uk].

Synthesis and Characterization of (1*R*,2*R*,4*S*)-*exo*-(2-Methoxy-3-trimethylsilylphenyl)-1,3,3-trimethylbicyclo[2.2.1]heptan-2-ol (3): A solution of *ortho*-lithioanisole in TMEDA/hexanes was prepared from *n*-butyllithium (0.11 mol, 1.59 M, 63 mL) in hexanes, TMEDA (0.11 mol, 16.5 mL) and anisole (0.10 mol, 10.9 mL).[24] Chlorotrimethylsilane (0.11 mol, 14.0 mL) was slowly added at 0 °C, and the reaction mixture was stirred at room temperature for 6 h. Hydrolytic workup ($NaHCO_3$ solution), washing, drying (Na_2SO_4), and distillation (1.0 mbar, 41 °C) yielded 12.8 g (71%) of 2-trimethylsilylanisole, which was added to a mixture of 45.7 mL *n*-butyllithium (80 mmol) in hexanes and 12.0 mL TMEDA (80 mmol) at 0 °C. (–)-Fenchone (70 mmol, 11.3 mL) was added at 0 °C and the mixture was stirred for 12 h at room temperature. Hydrolytic workup, washing, drying (Na_2SO_4) and crystallization at 6 °C yielded a crude product, which was recrystallized from pentane. White crystals of **3** were obtained (8.4 g, 25 mmol, 25%). M.p.: 104 °C. – $[\alpha]_D^{23}$ = –88.2 (*c* = 2.0, hexanes). – ^{1}H NMR (300 MHz, $CDCl_3$): δ = 0.32 [s, 9 H, (Si)CH_3], 0.49 (s, 3 H, CH_3), 1.11 (s, 3 H, CH_3), 1.16 (s, 3 H, CH_3), 1.10–2.45 (m, 7 H, $CH_{(2)}$), 3.82 (s, 3 H, (O)CH_3), 7.01 (t, ^3J = 7.6 Hz, 1 H, ar), 7.30 (d, ^3J = 7.2 Hz, 1 H, ar), 7.54 (d, ^3J = 8.0 Hz, 1 H, ar). – ^{13}C NMR ($CDCl_3$): δ = 0.6, 18.1, 21.7, 24.1, 29.7, 33.5, 41.6, 46.0, 49.6, 53.9, 64.4, 86.0, 122.0, 131.3, 132.8, 134.4, 135.4, 164.7. – IR (KBr, cm^{-1}): $\tilde{\nu}$ = 3465, 3045, 2954, 2866, 1012. – $C_{20}H_{32}O_2Si$ (332.56): calcd. C 72.23, H 9.70; found C 72.25, H 9.80. – X-ray crystal data of **3**: $C_{20}H_{32}O_2Si$; *M* = 332.56; space group $P2_1$; *a* = 7.6729(1) Å, *b* = 11.0159(2) Å, *c* = 11.4503(2) Å, β = 98.647(1)°; *V* = 956.82(3) Å^3; *Z* = 2; *T* = 200(2) K; μ = 0.131 mm^{-1}; reflections total: 7169, unique: 3178, observed: 3001 [$I > 2\sigma(I)$]; parameters refined: 219; R_1 = 0.029; wR_2 = 0.073; GOF_{all} = 1.04.

Synthesis and Characterization of (1*R*,2*R*,4*S*)-*exo*-(2-Dimethylaminomethyl-3-trimethylsilylphenyl)-1,3,3-trimethylbicyclo[2.2.1]heptan-2-ol (4): *ortho*-Lithio-*N*,*N*-dimethylbenzylamine was prepared from *n*-butyllithium (0.15 mol, 1.59 M, 94.3 mL) in hexanes and *N*,*N*-dimethylbenzylamine (0.15 mol, 22.53 mL).[24] Chlorotrimethylsilane (0.15 mol, 19.04 mL) was slowly added at 0 °C and the reaction mixture was stirred at room temperature for 6 h. Hydrolytic work up ($NaHCO_3$ solution), washing, drying (Na_2SO_4) and distillation (0.11 mbar, 52 °C) yielded 11.5 g (37%) of *N*,*N*-dimethyl-2-(trimethylsilyl)benzylamine, which was added to a mixture of *n*-butyllithium (55.7 mmol, 35 mL) in hexanes. The solution was stirred 1 h at 60 °C. (–)-Fenchone (55.7 mmol, 9.0 mL) was added at 0 °C and the mixture was stirred for 12 h at room temperature. Hydrolytic workup, washing, drying (Na_2SO_4) and crystallization at –30 °C yielded a crude product, which was recrystallized from pentane. White crystals of **4** were obtained (12.8 g, 36 mmol, 24%). M.p.: 115 °C. – $[\alpha]_D^{23}$ = –130.0 (*c* = 2.0, hexanes). – ^{1}H NMR (300 MHz, $CDCl_3$): δ = 0.32 [s, 9 H, (Si) CH_3], 0.33 (s, 3 H, CH_3), 1.14 (s, 3 H, CH_3), 1.18 (s, 3 H, CH_3), 2.18 [s, 6 H, (N)CH_3], 0.09–2.50 [m, 7 H, $CH_{(2)}$], 3.56 [d, 1 H, ^2J = 12 Hz, (N)CH_2], 4.03 [d, 1 H, ^2J = 12 Hz, (N)CH_2], 7.16 (t, 1 H, ^3J = 7.7 Hz, ar), 7.32 (d, 1 H, ^3J = 6.1 Hz, ar), 7.71 (d, 1 H, ^3J = 8.2 Hz, ar). – ^{13}C NMR ($CDCl_3$): δ = 2.1, 18.4, 23.6, 24.0, 29.6, 34.5, 41.4, 44.3, 46.7, 50.3, 54.5, 62.8, 86.1, 124.7, 132.1, 132.1, 141.0, 142.7, 144.6. – IR (KBr, cm^{-1}): $\tilde{\nu}$ = 3429, 3050, 2995, 2873, 2750, 1007. – $C_{22}H_{37}NOSi$ (359.63): calcd. C 73.48, H 10.37, N 3.89; found: C 73.45, H 10.36, N 3.91. – X-ray crystal data of **4**: $C_{22}H_{37}NOSi$; *M* = 359.63; space group $P2_1$; *a* = 9.9810(5) Å, *b* = 9.9875(5) Å, *c* = 11.3068(6) Å, β = 107.886(1)°; *V* = 1072.65(9) Å^3; *Z* = 2; *T* = 200(2) K; μ = 0.119 mm^{-1}; reflections total: 6840, unique: 3492, observed: 3345 [$I > 2\sigma(I)$]; parameters refined: 236; R_1 = 0.044; wR_2 = 0.114; GOF_{all} = 1.03.

Synthesis and Characterization of 3-Zn: A solution of dimethylzinc (0.4 mmol, 2.0 M, 0.2 mL) in toluene was added to **3** (0.4 mmol, 0.13 g) at 0 °C. The mixture was stirred for 1 h at room temperature (methane evolved). Colorless crystals of **3-Zn** were obtained by slow cooling of this solution to 0 °C. – – ^{1}H NMR (300 MHz, [D_8]toluene): δ = –0.16 [s, 3 H, (Zn)CH_3], 0.29 [s, 9 H, (Si)CH_3], 0.61 (s, 3 H, CH_3), 1.11–2.04 [m, 13 H, $CH_{(2,3)}$], 3.99 [s, 3 H, (O)CH_3], 6.82–7.60 (m, 3 H, ar). – ^{13}C NMR ([D_8]toluene): δ = –6.7, 1.4, 24.8, 25.0, 31.7, 35.4, 43.2, 48.1, 50.4, 56.4, 65.2, 91.5, 95.2, 122.7, 131.9, 133.6, 135.1, 139.3, 164.0. – $C_{42}H_{68}O_4Si_2Zn_2$ (823.88): calcd. C 62.03, H 8.52; found C 62.06, H 8.50. – X-ray crystal data of (**3-Zn**)$_2$: $C_{42}H_{68}O_4Si_2Zn_2$; *M* = 823.88; space group $P2_12_12_1$; *a* = 10.8060(1) Å, *b* = 16.0068(2) Å, *c* = 24.0982(3) Å; *V* = 4168.25(8) Å^3; *Z* = 4; *T* = 200(2) K; μ = 1.247 mm^{-1}; reflections total: 31055, unique:7277, observed: 6900 [$I > 2\sigma(I)$]; parameters refined: 467; R_1 = 0.021; wR_2 = 0.051; GOF_{all} = 1.05.

Catalysis: Catalysis was performed with ligands **1** to **4** according to the following general procedure: The ligand (0.07 mmol, 3 mol-% with respect to benzaldehyde) was treated with diethylzinc in hexanes (3.3 mL, 3 mmol, 0.9 M) at 0 °C for 15 min. To this mixture, benzaldehyde (0.24 mL, 0.25 g, 2.4 mmol) was added at the temperature specified for each ligand (Table 3). After the reaction time (24 h), the mixture was quenched with water and hydrolyzed with hydrochloric acid. The organic layer was separated, washed, neutralized ($NaHCO_3$), dried (Na_2SO_4) and 1-phenyl-1-propanol was distilled. The optical purity was measured by polarimetry and the enantiomeric excess was analyzed by chiral HPLC [Chiracel OB-H, 99.2:0.8 hexanes: *i*PrOH, 25 °C, 254 nm, 1-phenyl-1-propanol: 18.5 min (*S*), 25.6 min (*R*)].

Computational Details: The complexes and the transition structures were fully optimized without constraints with Morokuma's ONIOM[25] method implemented in GAUSSIAN98,[26] combining ab initio levels (RHF/LanL2DZ) with Rappe's universal force field

(UFF, Scheme 6).[27] LanL2DZ denotes Los Alamos ECP and double zeta basis set[28] for zinc and the Dunning-Huzinaga double zeta basis set[29] for the other elements. Hydrogen atoms were used as link atoms between the two layers (RHF/LanL2DZ:UFF). All transition structures were analyzed by frequency computations and showed one imaginary frequency of the methyl transfer mode.

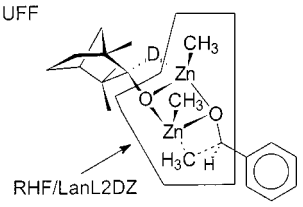

Scheme 6. ONIOM (RHF/LANL2DZ:UFF) layers of computed transition structures

Acknowledgments

We thank the Fonds der Chemischen Industrie (Liebig grant for B. G.), the Deutsche Forschungsgemeinschaft and the Research Pool Foundation (University Heidelberg) for financial support and the Degussa-Hüls AG for generous gifts of chemicals. B. G. is especially grateful to Prof. Dr. P. Hofmann for generous support at Heidelberg.

[1] For applications of organozinc reagents in organic synthesis see: [1a] P. Knochel, F. Langer, A. Longeneau, M. Rottländer, T. Stüdemann, *Chem. Ber.* **1997**, *130*, 1021–1027. – [1b] P. Knochel, R. D. Singer, *Chem. Rev.* **1993**, *93*, 2117–2188.

[2] [2a] A. Thompson, E. G. Corley, M. F. Huntington, E. J. J. Grabowski, J. F. Remenar, D. B. Collum, *J. Am. Chem. Soc.* **1998**, *120*, 2028–2038. – [2b] M. E. Pierce, R. L. Parsons, Jr., L. A. Radesca, Y. S. Lo, S. Silverman, J. R. Moore, Q. Islam, A. Choudhury, J. M. D. Fortunak, D. Nguyen, C. Luo, S. J. Morgan, W. P. Davis, P. N. Confalone, C. Chen, R. D. Tillyer, L. Frey, L. Tan, F. Xu, D. Zhao, A. S. Thompson, E. G. Corley, E. J. J. Grabowski, R. Reamer, P. J. Reider, *J. Org. Chem.* **1998**, *63*, 8536–8543.

[3] [3a] M. Arend, *Angew. Chem.* **1999**, *111*, 3047–3049; *Angew. Chem. Int. Ed.* **1999**, *38*, 2873–2874. – [3b] P. Brandt, C. Hedberg, K. Lawonn, P. Pinho, P. G. Andersson, *Chem. Eur. J.* **1999**, *5*, 1692–1699. – [3c] S. Kobayashi, H. Ishitani, *Chem. Rev.* **1999**, *99*, 1069–1094. – [3d] D. Enders, U. Reinhold, *Tetrahedron: Asymmetry* **1997**, *8*, 1895–1946.

[4] [4a] *Comprehensive Asymmetric Catalysis* (Eds.: E. N. Jacobsen, A. Pfaltz, H. Yamamoto), vol. I–III, Springer, Heidelberg, **1999**. – [4b] G. Helmchen, R. W. Hoffmann, J. Mulzer, E. Schaumann (Eds.), *Methods Org. Chem. (Houben-Weyl)*, **1996**, vol. E21b.

[5] For reviews see: [5a] K. Soai, S. Niwa, *Chem. Rev.* **1992**, *92*, 833–856. – [5b] R. Noyori, M. Kitamura, *Angew. Chem.* **1991**, *103*, 34–55; *Angew. Chem. Int. Ed. Engl.* **1991**, *30*, 49–69. – [5c] D. A. Evans, *Science* **1998**, *22*, 420–426.

[6] Ferrocenyl-hydroxy-oxazolines: [6a] C. Bolm, K. Muniz, *Chem. Commun.* **1999**, 1295–1296. – [6b] C. Bolm, K. Muniz-Fernandez, A. Seger, G. Raabe, K. Günther, *J. Org. Chem.* **1998**, *63*, 7860–7867. – Arene chromium ligands: [6c] C. Bolm, K. Muniz, *Chem. Soc. Rev.* **1999**, *28*, 51–59. – Titanium TADDOLates: [6d] P. B. Rheiner, D. Seebach, *Chem. Eur. J.* **1999**, *5*, 3221–3236. – [6e] B. Schmidt, D. Seebach, *Angew. Chem.* **1991**, *103*, 100–101; *Angew. Chem. Int. Ed. Engl.* **1991**, *30*, 99–101. – [6f] B. Schmidt, D. Seebach, *Angew. Chem.* **1991**, *103*, 1383–1385; *Angew. Chem. Int. Ed. Engl.* **1991**, *30*, 1321–1323.

[7] [7a] J. Eriksson, P. I. Arvidsson, O. Davidsson, *Chem. Eur. J.* **1999**, *5*, 2356–2361. – [7b] O. Juanes, J. C. Rodriguez-Ubis, E. Brunet, H. Pennemann, M. Kossenjans, J. Martens, *Eur. J. Org. Chem.* **1999**, 3323–3333.

[8] B. Goldfuss, K. N. Houk, *J. Org. Chem.* **1998**, *63*, 8998–9006.

[9] [9a] H.-U. Blaser, *Chem. Rev.* **1992**, *92*, 935–952. – [9b] M. Genov, K. Kostova, V. Dimitrov, *Tetrahedron: Asymmetry* **1997**, *8*, 1869–1876. – [9c] Y. Suzuki, Y. Ogata, K. Hiroi, *Tetrahedron: Asymmetry* **1999**, *10*, 1219–1222.

[10] [10a] M. Kitamura, S. Okada, S. Suga, R. Noyori, *J. Am. Chem. Soc.* **1989**, *111*, 4028–4036. – [10b] M. Kitamura, S. Suga, K. Kawai, R. Noyori, *J. Am. Chem. Soc.* **1986**, *108*, 6071–6072.

[11] [11a] G. Helmchen, *J. Organomet. Chem.* **1999**, *576*, 203–214. – [11b] A. Pfaltz, *Synlett* **1999**, 835–842. – [11c] J. M. J. Williams, *Synlett* **1996**, 705–710. – [11d] B. M. Trost, D. L. V. Vranken, C. Bingel, *J. Am. Chem. Soc.* **1992**, *114*, 9327–9343.

[12] Aminoarenethiolate ligands with similar benzylamino groups were successfully employed by the van Koten group in enantioselective diethylzinc additions: E. Rijnberg, N. J. Hovestad, A. W. Kleij, J. T. B. H. Jastrzebski, J. Boersma, M. D. Janssen, A. L. Spek, G. van Koten, *Organometallics* **1997**, *16*, 2847–2857.

[13] B. Goldfuss, M. Steigelmann, S. I. Kahn, K. N. Houk, *J. Org. Chem.*, **2000**, *65*, 77–82.

[14] For effects of trialkylsilyl substituents in palladium-catalyzed enantioselective rearrangements of allylic imidates and in cross-couplings see: [14a] Y. Donde, L. E. Overman *J. Am. Chem. Soc.* **1999**, *121*, 2933–3934. – [14b] J. M. Brown, M. Pearson, J. T. B. H. Jastrzebski, G. van Koten, *J. Chem. Soc., Chem. Commun.* **1992**, 1440–1441.

[15] The N7–C6–C5–C8 angle in the X-ray crystal structure of **4** (110°) is not increased relative to that in the X-ray crystal structure of **2** (110°) because close C6H–HCSi9 distances (H–H: 2.05 Å, C–C: 3.48 Å) favor a small N7–C6–C5–C8 dihedral angle in **4**. The repulsive C6H–HCSi9 contacts would decrease even more if N7–C6–C5–C8 increased to over 110°. Trimethylsilyl conformations analogous to that in the X-ray crystal structure of **4** were examined in transition structures with **4**, but were found to be energetically unfavorable.

[16] For correlations of ligand bite angles and catalyst reactivity see: [16a] P. Dierkes, P. W. N. M. van Leeuwen, *J. Chem. Soc., Dalton Trans.* **1999**, 1519–1529. – [16b] R. J. van Haaren, H. Oevering, B. B. Coussens, G. P. F. van Strijdonck, J. N. H. Reek, P. C. J. Kamer, P. W. N. M. van Leeuwen, *Eur. J. Inorg. Chem.* **1999**, 1237–1241.

[17] M. Kitamura, H. Oka, R. Noyori, *Tetrahedron* **1999**, *55*, 3605–3614.

[18] [18a] M. Kitamura, S. Suga, H. Oka, R. Noyori, *J. Am. Chem. Soc.* **1998**, *120*, 9800–9809. – [18b] M. Kitamura, M. Yamakawa, H. Oka, S. Suga, R. Noyori, *Chem. Eur. J.* **1996**, *2*, 1173–1181.

[19] B. Goldfuss, S. I. Kahn, K. N. Houk, *Organometallics* **1999**, *18*, 2927–2929.

[20] For both **1-Zn** and **3-Zn**, *syn* dimers were computed [ONIOM (RHF/LanL2DZ:UFF)] to be most stable and hence were considered for the monomer–dimer equilibrium; *anti* dimers, with *anti* aligned methyl groups at zinc centers, were computed to be 4.7 kcal/mol (**1-Zn**) and 3.4 kcal/mol (**3-Zn**) higher in energy.

[21] Attempts to obtain X-ray crystal structures of analogous methylzinc complexes of ligands **2** and **4** were not successful so far. No stable dimeric methylzinc complexes were found computationally for ligands **2** or **4**.

[22] Increased reactivity can lead to increased enantioselectivity, due to a smaller contribution of the slower, uncatalyzed racemic side reaction of diethylzinc with benzaldehyde. This, however, cannot explain the change in the direction of enantioselectivity for **3** relative to **1**.

[23] [23a] M. Yamakawa, R. Noyori, *J. Am. Chem. Soc.* **1995**, *117*, 6327–6335. – [23b] M. Yamakawa, R. Noyori, *Organometallics* **1999**, *18*, 128–133.

[24] L. Brandsma, H. Verkruijsse, *Preparative Polar Organometallic Chemistry*, Springer, Heidelberg, **1987**.

[25] S. Dapprich, I. Komaromi, K. S. Byun, K. Morokuma, M. J. Frisch, *Theochem.* **1999**, *461–462*, 1–21.

[26] M. J. Frisch, G. W. Trucks, H. B. Schlegel, G. E. Scuseria, M. A. Robb, J. R. Cheeseman, V. G. Zakrzewski, J. A. Montgomery, Jr., R. E. Stratmann, J. C. Burant, S. Dapprich, J. M. Millam, A. D. Daniels, K. N. Kudin, M. C. Strain, O. Farkas, J. Tomasi, V. Barone, M. Cossi, R. Cammi, B. Mennucci, C. Pomelli, C. Adamo, S. Clifford, J. Ochterski, G. A. Petersson, P. Y. Ayala, Q. Cui, K. Morokuma, D. K. Malick, A. D. Rabuck,

K. Raghavachari, J. B. Foresman, J. Cioslowski, J. V. Ortiz, B. B. Stefanov, G. Liu, A. Liashenko, P. Piskorz, I. Komaromi, R. Gomperts, R. L. Martin, D. J. Fox, T. Keith, M. A. Al-Laham, C. Y. Peng, A. Nanayakkara, C. Gonzalez, M. Challacombe, P. M. W. Gill, B. Johnson, W. Chen, M. W. Wong, J. L. Andres, C. Gonzalez, M. Head-Gordon, E. S. Replogle, J. A. Pople, *Gaussian 98, Revision A.5*, Gaussian, Inc., Pittsburgh, PA, **1998**.

[27] A. K. Rappé, C. J. Casewit, K. S. Colwell, W. A. Goddard III, W. M. Skiff, *J. Am. Chem. Soc.* **1992**, *114*, 10024–10035.

[28] P. J. Hay, W. R. Wadt, *J. Chem. Phys.* **1985**, *82*, 270.

[29] T. H. Dunning Jr., P. J. Hay, in *Modern Theoretical Chemistry* (Ed.: H. F. Schaefer III) Plenum, New York, **1976**, vol. 3, p. 1.

Received October 14, 1999
[O99570]